

Material-structure integrated design optimization of GFRP bridge deck on steel girder

Xin, Haohui; Mosallam, Ayman; Correia, José A.F.O.; Liu, Yuqing; He, Jun; Sun, Yun

DOI

[10.1016/j.istruc.2020.07.008](https://doi.org/10.1016/j.istruc.2020.07.008)

Publication date

2020

Document Version

Final published version

Published in

Structures

Citation (APA)

Xin, H., Mosallam, A., Correia, J. A. F. O., Liu, Y., He, J., & Sun, Y. (2020). Material-structure integrated design optimization of GFRP bridge deck on steel girder. *Structures*, 27, 1222-1230. <https://doi.org/10.1016/j.istruc.2020.07.008>

Important note

To cite this publication, please use the final published version (if applicable). Please check the document version above.

Copyright

Other than for strictly personal use, it is not permitted to download, forward or distribute the text or part of it, without the consent of the author(s) and/or copyright holder(s), unless the work is under an open content license such as Creative Commons.

Takedown policy

Please contact us and provide details if you believe this document breaches copyrights. We will remove access to the work immediately and investigate your claim.



Material-structure integrated design optimization of GFRP bridge deck on steel girder

Haohui Xin^{a,b,c}, Ayman Mosallam^d, José A.F.O. Correia^e, Yuqing Liu^{b,*}, Jun He^{f,g}, Yun Sun^b

^a School of Human Settlements and Civil Engineering, Xi'an Jiaotong University, Xi'an, China

^b Department of Bridge Engineering, Tongji University, Shanghai, China

^c Civil Engineering and Geosciences, Delft University and Technology, Netherlands

^d Department of Civil and Environment Engineering, University of California, Irvine, CA, USA

^e INEGI & CONSTRUCT, Faculty of Engineering, University of Porto, 4200-465 Porto, Portugal

^f School of Civil Engineering, Changsha University of Science and Technology, Changshang, China

^g Institute for Infrastructure and Environment, Heriot-Watt University, Edinburgh, UK

ARTICLE INFO

Keywords:

Composite bridge girder
Pultruded GFRP bridge deck
Laminations
Multiscale optimization

ABSTRACT

Design optimization of fiber-reinforced polymeric (FRP) composite products is essential to facilitate their applications in engineering structures. For bridge structures, the main design optimization goals are the reduction of FRP material consumption and the structure weight, which aim to reduce the initial construction cost and achieve a longer bridge span. Compared with conventional steel–concrete composite bridges, FRP-steel composite bridges possess more design variables and more complex design process, which necessitate the simplified optimization models. This paper aims to propose a two-scale design optimization method for FRP bridge deck on the steel girder. The macro behavior of the pultruded FRP composite bridge deck is analyzed. Regarding the micro level, the equivalent properties of pultruded GFRP lamination are calculated by combining micro-mechanics and classical lamination theory (CLT). The above-mentioned macro pultruded GFRP bridge level and the micro fiber/resin level were bridged based on the assumption that the micro-component effective homogenized strain equals to the corresponding macro strain. The two-scale lamination optimization of pultruded GFRP bridge deck is finally achieved by finding optimized two-scale design variables that can achieve the minimum bridge weight or the lowest initial construction cost with all listed constraint requirements satisfied. A pultruded FRP deck supported on equally-spaced steel girders was selected as a case study to show how to obtain the optimized two-scale parameters by using this proposed optimization method. The optimized results of the top flange thickness, t_w , the bottom flange thickness, t_b , the web height, h_w , and the web thickness per meter, t_w , are 46.02 mm, 45.86 mm, 300.0 mm and 37.42 mm, respectively. Results also showed that the optimized ratio of the 0°-lamina, 45°-lamina, and the 90°-lamina are 77.9%, 17.1%, 5.0%. The optimized fiber volume fraction is 65.2%.

1. Introduction

Fiber-reinforced polymer (FRP) composites have been greatly developed worldwide and have become one of the most popular construction materials for repair and rehabilitation and new construction [1–10]. Pultruded glass fiber reinforced polymer (GFRP) composites are great candidates for newly constructed bridges decks. A variety of GFRP bridge deck applications are presented in [11]. Fig. 1 shows a commonly used composite girder system which consists of the pultruded GFRP bridge deck and the supporting steel girders. Noted that the the steel girder with a corrugated web [12] is also an interesting surrogate.

The pultruded GFRP bridge decks and steel girders can be connected using adhesives or bolts [13].

Different from conventional isotropic construction materials like reinforced concrete and steel, GFRP composites are inhomogeneous and anisotropic, which require to be analyzed and designed on different scales, namely, the micro-scale and macro-scale. The importance of multi-scale analysis to determine the mechanical properties of GFRP materials has been pointed out in previous studies [14,15].

During the design stage of a GFRP bridge deck, engineers are not only interested in fulfilling the strength and serviceability requirements, which are the top design priorities, but also in satisfying these

* Corresponding author.

E-mail address: yql@tongji.edu.cn (Y. Liu).

<https://doi.org/10.1016/j.istruc.2020.07.008>

Received 4 June 2020; Received in revised form 27 June 2020; Accepted 4 July 2020

2352-0124/ © 2020 Institution of Structural Engineers. Published by Elsevier Ltd. All rights reserved.

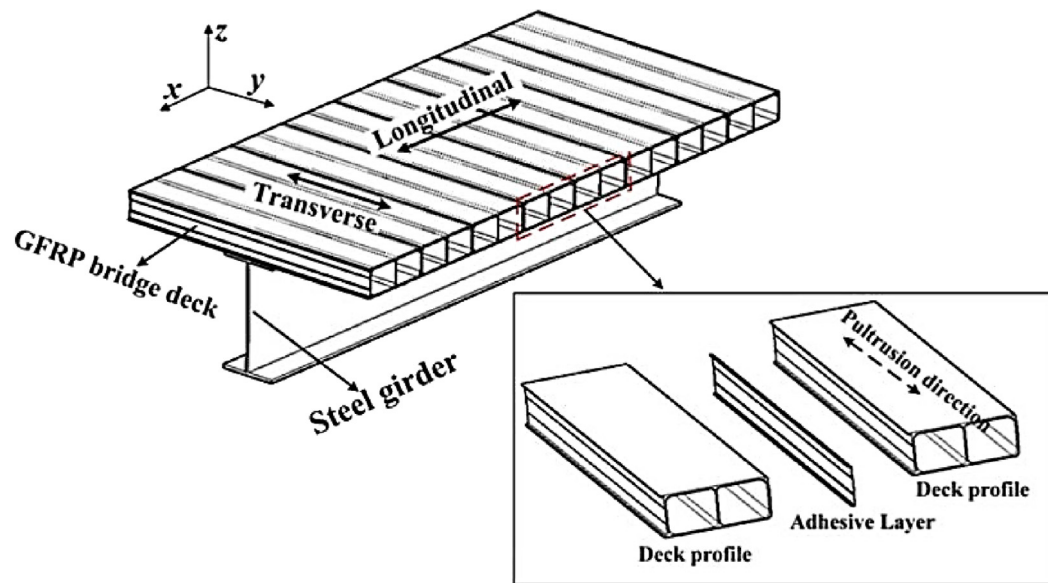


Fig. 1. Pultruded GFRP bridge deck and steel girder system [3].

requirements with the least possible amount of materials that will result in a weight reduction of the structure and further achieve lower initial construction cost. Thus optimization techniques is very important in obtaining the best use of FRP material in bridge decks. The optimization tasks involve determining the optimal ratio of fiber reinforcements, the optimum fiber volume fractions and geometric variables in order to achieve the best design in both material and structure scales. In addition, the complexity of general pultruded GFRP bridge decks necessitates the development of simplified optimization models.

Most of the previous optimization work in the design of composite structures [16–20] focused on aerospace structures, but pultruded GFRP composites, commonly used in bridge decks, are quite different in nature with the composites used in aerospace structures [15], as can be reflected in Fig. 2. These differences include: (i) the pultruded FRP laminations have a relatively poor quality, and (ii) the roving content is larger than fabrics, leading to an increase in the thickness of the unidirectional lamina (0°-lamina) of up to 5–15 times the laminas with other orientations.

A pilot investigation related to material-structure integrated design is presented in this paper. The macro behavior of the pultruded FRP

composite bridge deck is analyzed. Regarding the micro level, the equivalent properties of pultruded GFRP lamination are calculated by combining micromechanics and classical lamination theory (CLT). The above-mentioned macro pultruded GFRP bridge deck level and the micro fiber/resin level were bridged based on the assumption that the micro-component effective homogenized strain equals to the corresponding macro strain. The two-scale lamination optimization of pultruded GFRP bridge deck is finally achieved by finding optimized two-scale design variables that can achieve the minimum bridge weight or the lowest initial construction cost with all listed constraint requirements satisfied. Also, a case study was presented to show how to obtain the optimized two-scale parameters by adopting the proposed optimization method in the last part of this paper.

2. Macro behaviour of the pultruded GFRP composite bridge deck

GFRP composite bridge decks, together with the supporting steel girders, were subjected to longitudinal bending moment (M^L) and shear force (Q^L), as well as transverse bending moment (M^T) and shear force (Q^T). The following sections would describe the mechanical behaviors of bridge deck in both the longitudinal and transverse directions under corresponding bending moment and shear force.

2.1. Macro behavior in the longitudinal direction

Following assumptions were made to analyze the mechanical behavior of the composite girder along longitudinal direction: (i) the shear connection stiffness is sufficient to ensure a full composite action between the GFRP bridge deck and the supporting steel girder; (ii) the longitudinal shear forces are fully resisted by the steel webs; (iii) the macro longitudinal stresses are uniformly distributed along the flange thickness considering the fact that the laminate thickness dimension is quite small relative to the total height of the steel girder; (iv) the flexural and shear resistances provided by discontinuous web along the longitudinal direction are neglected.

Due to the in-plane shear flexibility of the GFRP composite deck, the normal stress along the width of the deck is non-uniformly distributed, see Fig. 3. The maximum stress in the deck occurs in the centerline of the web and stresses in the bridge deck away from the web lag behind [21]. Thus, the effective flange width, b_{eff} , is introduced in design practice to simplify the analytical procedure, as denoted in Fig. 3. The effective flange width, b_{eff} , is defined as a reduced width of the deck

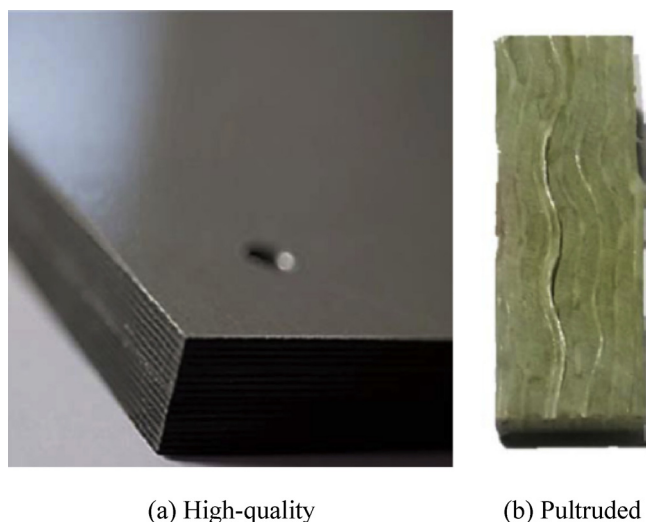


Fig. 2. Difference in quality and accuracy of stacking sequence of composite laminates [15].

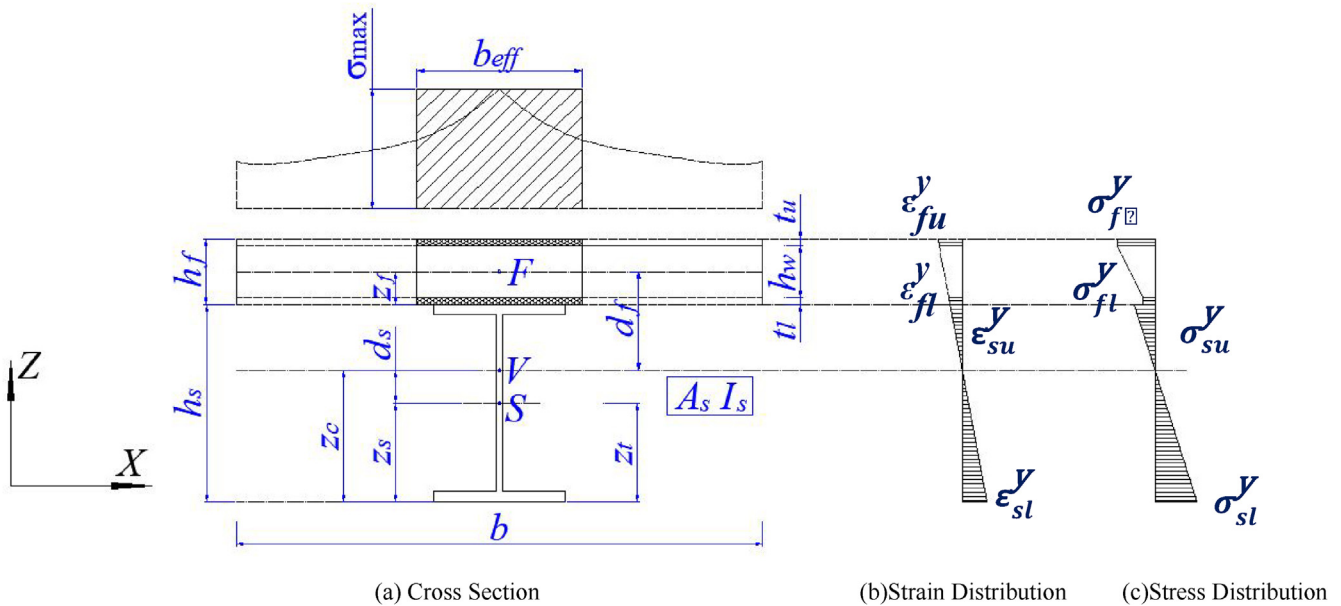


Fig. 3. Schematic of composite cross section.

over which the normal stresses are assumed to be uniformly distributed, and it is calculated [22,23] based on the premise that the stress resultant over the effective width should be equal to the stress resultant over the actual flange width, as defined in Eq. (1).

$$b_{eff} = \frac{\int_0^b \sigma_f^L(x) dx}{(\sigma_f^L)_{max}} \quad (1)$$

where: $\sigma_f^L(x)$ is longitudinal normal stress in the flange of GFRP bridge deck; $(\sigma_f^L)_{max}$ is the maximum longitudinal normal stress in the flange of GFRP bridge deck, and b is the center-to-center spacing of the steel girders.

The effective flange width of the GFRP bridge deck supported by the steel girders can be simply predicted [22] by using Eqs. (2) and (3) as follows:

$$b_{eff} = R b_{eff,s} \quad (2)$$

$$R = 1.025(1 - 0.0244^\vartheta) \quad (3)$$

where: $b_{eff,s}$ is the effective width suggested by highway bridges design specifications [30,31], and ϑ is the degree of composite action between the GFRP composite bridge deck and the main girders. The longitudinal normal stresses at the top flange, σ_{fu}^y , and the bottom flange, σ_{fl}^y , can be calculated by Eqs. (4) and (5) as follows:

$$\sigma_{fu}^y = -\frac{M^L z_{fu}^L}{n I_v} \quad (4)$$

$$\sigma_{fl}^y = -\frac{M^L z_{fl}^L}{n I_v} \quad (5)$$

where: n is the elastic moduli ratio (modular ratio) between steel modulus (E_s) and the longitudinal modulus of the GFRP composites deck (E_f^y) and is expressed by Eq. (6):

$$n = \frac{E_s}{E_f^y} \quad (6)$$

z_{fu}^L and z_{fl}^L are the distances from the top and the bottom flanges of the GFRP deck to the neutral axis of the GFRP/steel composite girder, z_c , respectively. Thus:

$$z_{fu}^L = h_s + t_l + h_w + t_u/2 - z_c \quad (7)$$

$$z_{fl}^L = h_s + \frac{t_l}{2} - z_c \quad (8)$$

The distance between the neutral axis of the GFRP/steel composite girder and the bottom fiber of the steel girder, z_c , is calculated by the following equation:

$$z_c = \frac{2A_s E_s z_s + b_{eff} E_f^y (t_l^2 + t_u^2 + 2t_u h_w + 2t_u t_l + 2t_u h_s + 2h_s t_l)}{2(A_s E_s + b_{eff} t_u E_f^y + b_{eff} t_l E_f^y)} \quad (9)$$

The equivalent moment of inertia of the GFRP/steel composite girder I_v could be calculated by Eq. (10).

$$I_v = I_s + A_s (z_c - z_s)^2 + b_{eff} (t_u^3 + t_l^3)/(12n) + b_{eff} (t_u + t_l)(h_s + z_f - z_c)^2 / n \quad (10)$$

$$z_f = \frac{t_l^2 + t_u^2 + 2t_u h_w + 2t_u t_l}{2(t_l + t_u)} \quad (11)$$

where: h_s is the height of the steel beam; t_l is the thickness of bottom flange; t_u is the thickness of the top flange; h_w is the web height of pultruded GFRP bridge deck; A_s is the cross-sectional area of the steel beam, and z_s is the distance between the neutral axis and the bottom fiber of the steel girder.

2.2. Macro behavior in the transverse direction

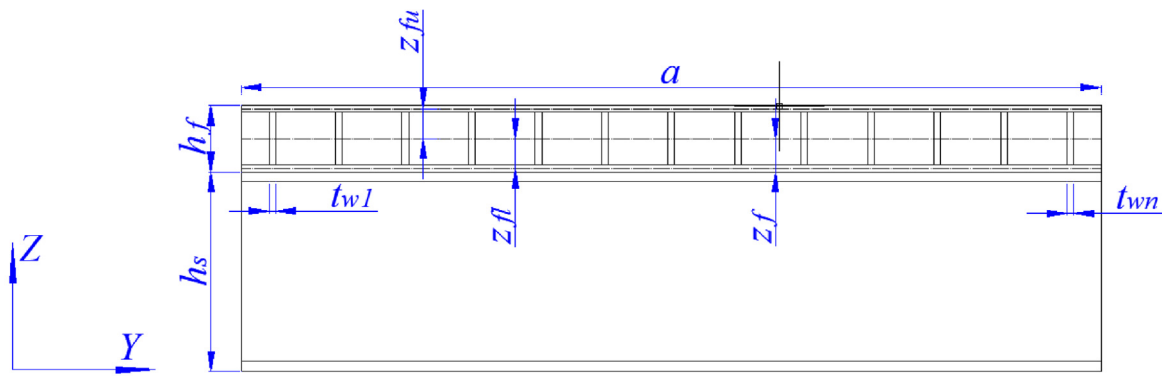
The following assumptions were made to analyze the longitudinal mechanical behavior of the GFRP-steel composite girder: (i) the transverse shear force is fully resisted by the web of GFRP bridge deck; (ii) the transverse normal stress is uniformly distributed along with the top/bottom flange thickness.

The transverse normal stress in the top flange σ_{fu}^x and bottom flange σ_{fl}^x , as denoted in Fig. 4, could be calculated based on Eqs. (12) and (13).

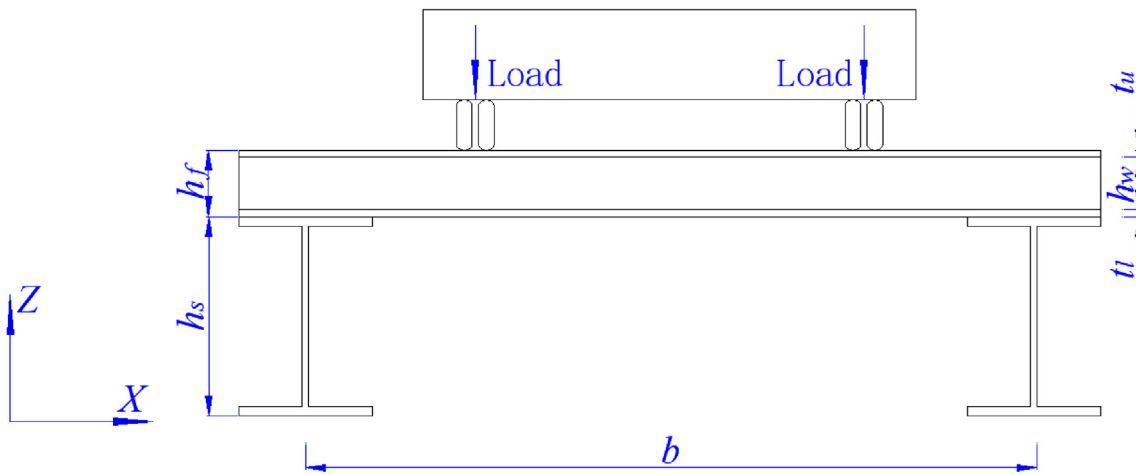
$$\sigma_{fu}^x = -\frac{M^T z_{fu}^T}{I_f^x} \quad (12)$$

$$\sigma_{fl}^x = \frac{M^T z_{fl}^T}{I_f^x} \quad (13)$$

where: the transverse moment of inertia I_f^x of pultruded GFRP bridge



(a) Geometry symbols in YZ plane



(b) Geometry symbols in XZ plane

Fig. 4. GFRP/Steel composite bridge girder parameters.

deck is:

$$I_f^x = \frac{1}{12}(1000 t_u^3 + 1000 t_l^3 + t_w h_w^3) + 1000 t_u (z_{fu}^T)^2 + 1000 t_l (z_{fl}^T)^2 + t_w h_w (z_{fw}^T)^2 \quad (14)$$

Note positive and negative signs in Eqs. (12) and (13) represent tensile and compressive stresses, respectively.

The web thickness per meter t_w along longitudinal direction is calculated by Eq. (15).

$$t_w = \frac{1000}{a} \sum_i^n t_{w(i)} \quad (15)$$

where, a is the width of GFRP deck profile, and $t_{w(i)}$ is the thickness of web in each GFRP deck profile.

z_{fu}^T in Eq. (11) and z_{fl}^T in Eq. (12) respectively refers to the distances between the top/bottom flange of GFRP composite bridge deck and its neutral axis, and can be calculated by Eqs. (16) and (17), respectively:

$$z_{fu}^T = t_l + h_w + t_u - z_f^T \quad (16)$$

$$z_{fl}^T = z_f^T \quad (17)$$

where the height of the GFRP bridge deck neutral axis along the

transverse direction, z_f^T , is given by Eq. (18):

$$z_f^T = \frac{1000(t_u t_l + t_u h_w) + h_w t_w (t_l + h_w/2) + 500(t_l^2 + t_u^2)}{1000 t_u + h_w t_w + 1000 t_l} \quad (18)$$

The shear stress, τ_{fw}^{xy} in the web of the pultruded GFRP bridge deck is calculated by Eq. (19):

$$\tau_{fw}^{xy} = \frac{Q^T}{t_w h_w} \quad (19)$$

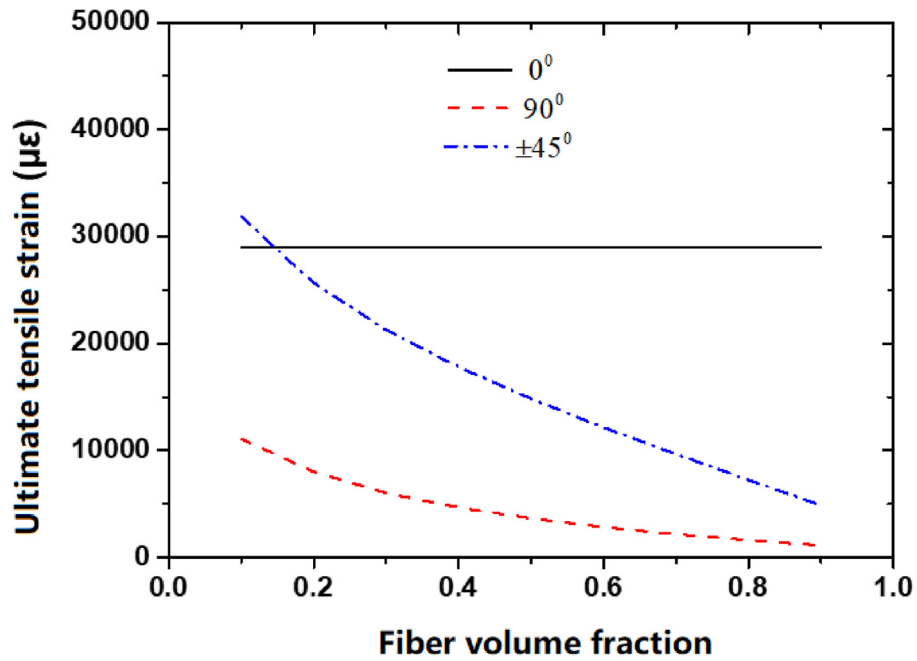
In order to guarantee a safe design, the GFRP bridge deck is assumed simply supported by steel girder. The transverse deflection of pultruded GFRP bridge deck can be conservatively predicted using Timoshenko beam theory [25]:

$$\delta_f^{z(\max)} = \frac{5M^T b^2}{48 E_f^x I_f^x} + \frac{Q^T b}{4 t_w h_w G_f^{xy}} \quad (20)$$

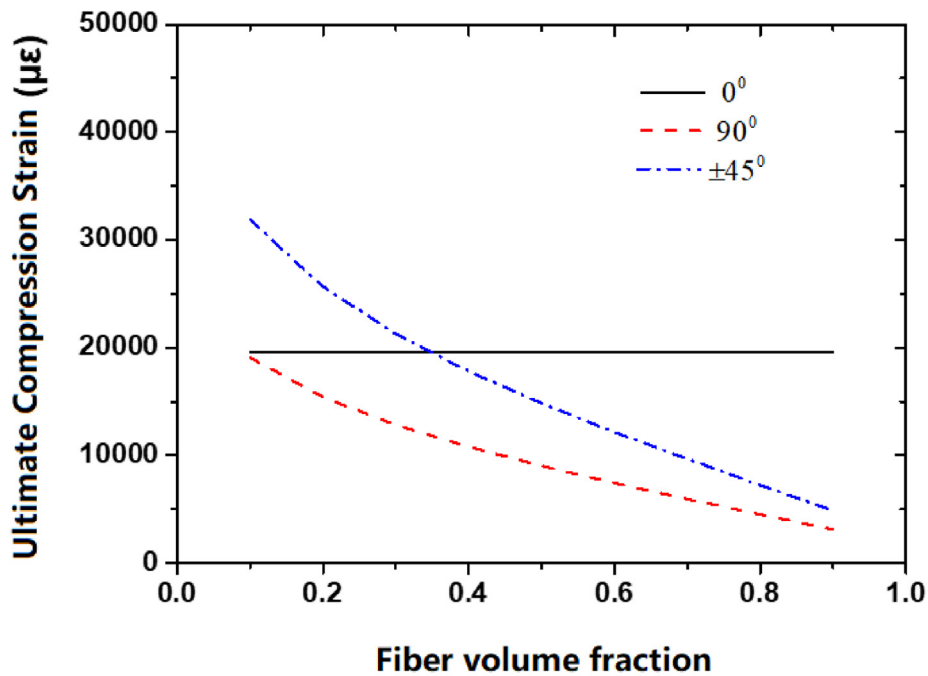
where: E_f^x and G_f^{xy} are the elastic and in-plane shear moduli of the GFRP composite bridge deck in the transverse direction.

3. Micro behavior of pultruded lamination

The reinforcements used for manufacturing the pultruded GFRP



(a) Tension



(b) Compression

Fig. 5. Ultimate strain variation of FRP lamina in relation to fiber volume fraction.

composite bridge deck described in this paper are composed of (i) unidirectional E-glass roving, and (ii) non-crimp (multi-warp knitted) fabrics [15]. In general, the laminations lay-up includes three different types of the lamina, namely, 0°-plies in the form of E-glass roving, and non-crimp E-glass fabrics with 90° and ±45° orientations. Based on the classical lamination theory [26], the effective modulus of the pultruded laminate could be estimated using Eqs. (21)–(23), assuming that the

ratio of 0°, 45°, and 90° lamina to the total lamination are ξ_0 , ξ_{45} , and ξ_{90} , respectively.

$$E_f^x = \xi_0 \left[\frac{E_1 - \nu_{12}^2 E_2}{1 - \nu_{12} \nu_{21}} \right] + \xi_{90} \left[\frac{E_1 E_2 - \nu_{12}^2 E_2^2}{E_1 (1 - \nu_{12} \nu_{21})} \right] + \xi_{45} \frac{1}{(1 - \nu_{12} \nu_{21})} \left[\frac{(E_1 + E_2 + 2\nu_{12} E_2 + 4(1 - \nu_{12} \nu_{21}) G_{12})^2 - 16(\nu_{12} E_2)^2}{4[E_1 + E_2 + 2\nu_{12} E_2 + 4(1 - \nu_{12} \nu_{21}) G_{12}]} \right] \quad (21)$$

Table 1
Mechanical properties of E-glass fibers [15].

Longitudinal modulus (E_{f1})	Transverse modulus (E_{f2})	Poisson's ratio (ν_f)	Shear modulus (G_f)	Tensile strength (X_{ft})	Compressive strength (X_{fc})	Density (ρ)
74.0 GPa	74.0 GPa	0.20	30.80 GPa	2150 MPa	1450 MPa	2560 kg/m ³

Table 2
Mechanical properties of epoxy resin [15].

Modulus (E_m)	Poisson's ratio (ν_m)	Shear modulus (G_m)	Tensile strength (X_{mt})	Compressive strength (X_{mc})	Shear strength (S_m)	Density (ρ)
3.35 GPa	0.35	1.24 GPa	80 MPa	120 MPa	75 MPa	1160 kg/m ³

$$E_f^y = \xi_0 \left[\frac{E_1 E_2 - \nu_{12}^2 E_2^2}{E_1 (1 - \nu_{12} \nu_{21})} \right] + \xi_{90} \left[\frac{E_1 - \nu_{12}^2 E_2}{1 - \nu_{12} \nu_{21}} \right] + \xi_{45} \frac{1}{(1 - \nu_{12} \nu_{21})} \left[\frac{(E_1 + E_2 + 2\nu_{12} E_2 + 4(1 - \nu_{12} \nu_{21}) G_{12})^2 - 16(\nu_{12} E_2)^2}{4[E_1 + E_2 + 2\nu_{12} E_2 + 4(1 - \nu_{12} \nu_{21}) G_{12}]} \right] \quad (22)$$

$$G_f^{xy} = \xi_0 G_{12} + \xi_{90} G_{12} + \xi_{45} \left[\frac{E_1 + E_2 - 2\nu_{12} E_2}{4(1 - \nu_{12} \nu_{21})} \right] \quad (23)$$

where: E_f^x is the effective elastic modulus of GFRP laminates in the longitudinal direction of the bridge; E_f^y is the effective elastic modulus of GFRP laminates in the transverse direction of the bridge; G_f^{xy} is the effective in-plane shear modulus of GFRP laminates.

The longitudinal modulus, E_1 , transverse modulus, E_2 , shear modulus, G_{12} , and Poisson's ratio, ν_{12} of the lamina can be determined based on the modified mixture formulae [6]:

$$E_1 = E_{f1} V_f + E_m V_m \quad (24)$$

$$E_2 = \frac{E_{f2} E_m [V_f \eta_2 V_m]}{E_m V_f + E_{f2} \eta_2 V_m} \quad (25)$$

$$\eta_2 = \frac{0.2}{1 - \nu_m} \left(1.1 - \sqrt{\frac{E_m}{E_{f1}}} + \frac{3.5 E_m}{E_{f1}} \right) (1 + 0.22 V_f) \quad (26)$$

$$G_{12} = \frac{G_f G_m (V_f + \eta_{12} V_m)}{G_m G_f + G_f + \eta_{12} V_m} \quad (27)$$

$$\eta_{12} = 0.28 + \sqrt{\frac{E_m}{E_f}} \quad (28)$$

$$\nu_{12} = \nu_f V_f + \nu_m V_m \quad (29)$$

where: E_{f1} is the longitudinal elastic modulus of fiber, E_{f2} is the transverse elastic modulus of fiber, V_f is the fiber volume fraction, ν_f is the fibers' Poisson's ratio, E_m is the matrix elastic modulus, V_m is the resin volume fraction, ν_m is the matrix's Poisson's ratio, G_f is the shear modulus of fibers, and G_m is the resin shear modulus.

The strength-based design method is accepted in many design practices, however, in this study, the variation of elastic moduli and ultimate strength of each lamina complicates the lamination optimization procedures. Thus, the strain-based design method is adopted in this paper.

By neglecting the curvature effects, the ultimate strain of each ply in the laminate is deemed to be the same based on First-Ply-Failure (FPF) analytical method [26]. The ultimate strain of each lamina can be obtained based on the micromechanics approach [6] using Eqs. (30)–(34).

$$t\epsilon_1^u = \frac{X_{ft}}{E_1} = \frac{X_{ft}}{E_{f1}} = t\epsilon_f^u \quad (30)$$

$$c\epsilon_1^u = \frac{X_{fc}}{E_1} = \frac{X_{fc}}{E_{f1}} = c\epsilon_f^u \quad (31)$$

$$t\epsilon_2^u = \frac{Y_T}{E_2} = \frac{X_{mt} (E_m V_f + E_{f2} \eta_2 V_m)}{SCF E_{f2} E_m (V_f + \eta_2 V_m)} \quad (32)$$

$$c\epsilon_2^u = \frac{Y_C}{E_2} = \epsilon_{mc} \left[1 - (4V_f/\pi) \left(1 - \frac{E_m}{E_{f2}} \right) \right] \quad (33)$$

$$u\gamma_{12} = \frac{S}{G_{12}} = S_m \left[1 + (V_f - \sqrt{V_f}) \left(1 - \frac{G_m}{G_f} \right) \right] \frac{(G_m V_f + G_f \eta_{12} V_m)}{G_f G_m (V_f + \eta_{12} V_m)} \quad (34)$$

When applying loads along the pultrusion direction, the ultimate strain of the 0°, 90°, ±45° lamina is ϵ_1^u , ϵ_2^u , and $u\gamma$, respectively. When the loads are applied perpendicular to the pultrusion direction, the ultimate strain of 0°, 90°, ±45° lamina is ϵ_2^u , ϵ_1^u and $u\gamma$, respectively. Based on the “First-Ply-Failure” failure criterion, the ultimate strain of each lamina can be calculated using Eqs. (35)–(37). The ultimate strain variation as related to fiber volume fraction is shown in Fig. 5. These values were calculated using Eqs. (31)–(37) with material properties listed in Tables 1 and 2 [27].

$$t\epsilon^u = \min(t\epsilon_1^u, t\epsilon_2^u, u\gamma) = t\epsilon_2^u \quad (35)$$

$$c\epsilon^u = \min(c\epsilon_1^u, c\epsilon_2^u, u\gamma) = c\epsilon_2^u \quad (36)$$

$$\gamma^u = \gamma_{12}^u \quad (37)$$

4. Design values

In general, bridge structural members are exposed to harsh and changing environments such as moisture, salt-spray agents, freeze–thaw cycles, and large variations in both temperature and humidity [28–32]. Due to continuous exposure to such harsh environments, degradation in the mechanical properties of composites is expected to occur [28–32]. In this section, the assumption was made that the design strain equals to the product of ultimate strain and a reduction or a degradation coefficient. For the top flange of a pultruded GFRP composite bridge deck, we have:

$$\begin{cases} |\bar{\epsilon}_{fu}^x| \leq c\epsilon^d \approx c\chi_d c\epsilon^u \\ |\bar{\epsilon}_{fu}^y| \leq c\epsilon^d \approx c\chi_d c\epsilon^u \end{cases} \quad (38)$$

for the bottom flange of pultruded GFRP bridge deck, we have:

$$\begin{cases} |\bar{\epsilon}_{fl}^x| \leq t\epsilon^d \approx t\chi_d t\epsilon^u \\ |\bar{\epsilon}_{fl}^y| \leq c\epsilon^d \approx c\chi_d c\epsilon^u \end{cases} \quad (39)$$

and for the web of pultruded GFRP bridge deck, we have:

$$|\bar{\gamma}_w^{xy}| \leq s\gamma^d \approx s\chi_d s\gamma^u \quad (40)$$

where: χ_d , $t\chi_d$, $s\chi_d$ are the reduction (degradation) coefficients for GFRP materials in compression, in tension, and in shear, respectively.

The Chinese Technical Code for Infrastructure Application of FRP Composites (GB 50608–2010) [32] suggests that the design values are determined by dividing experimental ultimate strength by appropriate partial safety factors that account for material type, and the surrounding environment. The following equations can be used to calculate the reduction (degradation) coefficient:

$$\chi_d = \frac{\mu^u - 1.645\sigma}{\mu^u} \frac{1}{\gamma_f \gamma_e} \tag{41}$$

where: μ^u is the average material strength; σ is the standard derivation of the test number; γ_f is the partial safety factor to account for material type; γ_e is the partial safety factor to account for environmental exposure.

In addition, the transverse deflection of the pultruded GFRP bridge deck should always be smaller than a limiting transverse deflection to ensure the stiffness requirement.

$$\delta_f^{z(\max)} \leq \delta^u \tag{42}$$

where: $\delta_f^{z(\max)}$ is the maximum transverse deflection of GFRP bridge deck under applied load, δ^u is the limited transverse deflection based on the design requirement.

5. Bridging fiber/resin level to structure level

In this section, the micro fiber/resin scale is bridged to the macro the GFRP/steel composite girder scale by assuming that the effective homogenized strain obtained from micro-component equals to macro-strain. Linking micro and macro longitudinal and transverse strains at the top flange of a pultruded GFRP bridge deck is achieved by using the following equations:

$$\bar{\epsilon}_{fu}^x = \frac{\bar{\sigma}_{fu}^x}{E_f^x} \approx -\frac{M^T z_{fu}^T}{E_f^x I_f^x} \tag{43}$$

$$\bar{\epsilon}_{fu}^y = \frac{\bar{\sigma}_{fu}^y}{E_f^y} \approx -\frac{M^L z_{fu}^L}{n I_v E_f^y} \tag{44}$$

Similarly, linking both micro and macro longitudinal and transverse strains at the bottom flange of a pultruded GFRP bridge deck is achieved by the following equations:

$$\bar{\epsilon}_{fl}^x = \frac{\bar{\sigma}_{fl}^x}{E_f^x} \approx \frac{M^T z_{fl}^T}{E_f^x I_f^x} \tag{45}$$

$$\bar{\epsilon}_{fl}^y = -\frac{M^L z_{fl}^L}{n I_v E_f^y} \tag{46}$$

Eq. (48) shows how to link the micro and macro shear strains at the web of a pultruded GFRP bridge deck:

$$\bar{\gamma}_w^{xy} = \frac{\bar{\tau}_w^{xy}}{G_f^{xy}} = \frac{Q^T}{t_w h_w G_f^{xy}} \tag{47}$$

6. Optimization equations for pultruded bridge decks

The main goals of multiscale optimization of GFRP bridge decks towards material-structure integrated design are to achieve: (i) the lightest weight to increase the bridge span while satisfying all design and manufacturing requirements, or (ii) the lowest cost for the economy and constructional convenience. Mathematically speaking, the multiscale optimization of GFRP bridge decks is to seek a minimum value of cost or weight by optimizing multiscale design variables within given allowed constrained functions determined by design and manufacturing requirements. In this paper, the multiscale lamination optimization of a pultruded GFRP bridge deck is achieved by finding an optimized two-scale design variable vector, \mathbf{x} , that drive the objective weight function, ϕ_1 , or the objective price function, ϕ_2 , to its lowest values while satisfying all constraint functions ($\phi^1 \sim \phi^6$). The design variables, objective functions, and constraint functions will be explained in the following sections.

(1) Design Variables: Eq. (48) describes the two-scale optimization design variable vector, \mathbf{x} , including the thickness of the top flange, t_u , the thickness of the bottom flange, t_l , the height of the web, h_w , the

thickness per meter of the web, t_w , the ratio of 0°, 45°, 90° lamina to the total laminate are $\xi_0, \xi_{45},$ and $\xi_{90},$ respectively, and the fiber volume fraction V_f .

$$\mathbf{x} = [t_u, t_l, h_w, t_w, \zeta_0, \zeta_{90}, \zeta_{45}, V_f]^T \tag{48}$$

(2) Objective function: The objective function ϕ_1 related to the optimizing weight is given as follows:

$$\phi_1 = 1000[1000(t_u + t_l) + h_w t_w](\rho_f V_f + \rho_m V_m) \tag{49}$$

where: ρ_f is fiber density, and ρ_m is the resin density.

The objective function, ϕ_2 , related to the optimizing cost is given in Eqn. (50). It should be noted that the manufacturing cost is not included in this expression due to the fact that different manufacturers have different selling prices.

$$\phi_2 = 1000[1000(t_u + t_l) + h_w t_w](\eta_f \rho_f V_f + \eta_m \rho_m V_m) \tag{50}$$

where: η_f is the price of the fibers, and η_m is the price of the matrix.

(3) Constraint functions: In this study, a total of six constraint functions were specified as follows.

(i) Constraint function Φ^1 (strength requirement of the top flange):

The longitudinal and transverse normal strains at the top flange of the GFRP deck should be smaller than corresponding design values of normal strains, i.e.,

$$\Phi^1 = \begin{cases} |\bar{\epsilon}_{fu}^x| \leq t e^d \\ |\bar{\epsilon}_{fu}^y| \leq c e^d \end{cases} \tag{51}$$

(ii) Constraint function Φ^2 (strength requirement of the bottom flange):

The longitudinal and transverse normal strains at the bottom flange of the GFRP deck should be smaller than corresponding allowable maximum normal strains, i.e.,

$$\Phi^2 = \begin{cases} |\bar{\epsilon}_{fl}^x| \leq t e^d \\ |\bar{\epsilon}_{fl}^y| \leq c e^d \end{cases} \tag{52}$$

(iii) Constraint function Φ^3 (strength requirement of the web):

The shear strain at the web of the GFRP deck should be smaller than allowable maximum shear strain, i.e.,

$$\Phi^3 = |\bar{\gamma}_w^{xy}| \leq s \gamma^d \tag{53}$$

(iv) Constraint function Φ^4 (stiffness requirement):

The transverse displacement of the GFRP deck should be smaller than the specified deflection, i.e.:

$$\Phi^4 = \delta_f^{z(\max)} \leq \delta^u \tag{54}$$

(v) Constraint function Φ^5 (manufacturing requirement):

The fractions of different types of laminates should be within the specified ranges, which are determined by the pultrusion manufacture, i.e.:

$$\Phi^5 = \begin{cases} 0.25 \leq V_f \leq 0.75 \\ \xi_0^l \leq \xi_0 \leq \xi_0^h \\ \xi_{45}^l \leq \xi_{45} \leq \xi_{45}^h \\ \xi_{90}^l \leq \xi_{90} \leq \xi_{90}^h \end{cases} \tag{55}$$

(vi) Constraint function Φ^6 (geometrical requirement):

The thickness of the plates should be within the specified ranges to avoid local buckling occurring in the excessive thin plate, and to meet the manufacturing capabilities since each manufacturer can only produce the GFRP plate within the specific range of the thickness, i.e.:

$$\Phi^6 = \begin{cases} (t_u)^l \leq t_u \leq (t_u)^u \\ (t_l)^l \leq t_l \leq (t_l)^u \\ (t_w)^l \leq t_w \leq (t_w)^u \\ (h_w)^l \leq h_w \leq (h_w)^u \end{cases} \quad (56)$$

7. Application to composite bridge girder

A composite bridge girder with a main span of 20.0 m was selected for a case study. This bridge girder consists of GFRP bridge decks and I-shaped steel girders with equal center-to-center spacing of 3.0 m. The GFRP composite deck is connected to steel girders using the bolted connector, and the degree of composite action between GFRP bridge deck and steel girder, η is specified as 0.72. The total height of the I-shaped steel girder is 1000 mm, the thickness of the top flange, bottom flange, and the web, are, 20.0 mm, 25.0 mm, and 20.0 mm, respectively, and the width of both the top and bottom flanges is 400.0 mm. According to the Chinese bridge specifications [24], the design load was calculated as:

$$S_{ud} = \sum_{i=1}^m \gamma_{Gi} S_{Gik} + \gamma_{Q1} S_{Q1k} + \varphi_c \sum_{j=2}^n \gamma_{Qj} S_{Qjk} \quad (57)$$

where: γ_{Gi} , γ_{Q1} , γ_{Qj} is the partial safety factor to dead load, vehicle load and live load excluding vehicle load; S_{Gik} , S_{Q1k} , S_{Qjk} represent the load effects, resulting from the dead load, vehicle load, and live load excluding vehicle load, respectively; and φ_c is the combination reduction parameter for the load effect resulting from the live load excluding vehicle load. Note that the design load S_{ud} can refer to different types of load effects, such as bending moment or shear force. In this study, the design loads include longitudinal bending moment M^L , longitudinal shear force, Q^L , transverse bending moment, M^T , and transverse shear force, Q^T , and they were computed based below equation:

$$M^L = \frac{1.1[1.2(q_{s1} + Lq_{f1} + bq_{G2}) + 1.4(1 + \mu)q_{Q1} + 1.12bq_{Q2}]L^2}{8} + \frac{(1 + \mu)^L P_{Q1} L}{4} \quad (58)$$

$$Q^L = \frac{1.1[1.2(q_{s1} + Lq_{f1} + bq_{G2}) + 1.4(1 + \mu)q_{Q1} + 1.12bq_{Q2}]L}{2} + \frac{1.2(1 + \mu)^L P_{Q1}}{2} \quad (59)$$

$$M^T = \frac{1.1[1.2(Tq_{f1} + 1000q_{G2}) + 1120q_{Q2}]b^2}{8} + \frac{1.4(1 + \mu)TP_{Q1}b}{4} \quad (60)$$

$$Q^T = \frac{1.1[1.2(Tq_{f1} + 1000q_{G2}) + 1120q_{Q2}]b}{2} + \frac{1.4(1 + \mu)^T P_{Q1}}{2} \quad (61)$$

where Lq_{f1} and Tq_{f1} is the self-weight of GFRP deck along the longitudinal and transverse direction respectively; q_{s1} is the self-weight of steel girder; q_{G2} is the self-weight of paving, defined as 5 kN/m³; q_{Q1} is the line load of the vehicle, defined as 10.5 kN/m * b/3000; P_{Q1} is the concentration load of the vehicle, defined as 280kN*b/3000; μ is impact coefficient, defined as 0.3.

The objective function of weight, ϕ_1 , is specified as:

$$\phi_1 = 1000[1000(t_u + t_l) + h_w t_w][1.28 \times 10^{-5} V_f + 3.25 \times 10^{-5}(1 - V_f)] \quad (62)$$

while the objective function of price, ϕ_2 , is specified as:

$$\phi_2 = 1000[1000(t_u + t_l) + h_w t_w][2.56 \times 10^{-6} V_f + 1.16 \times 10^{-6}(1 - V_f)] \quad (63)$$

The reduction (degradation) coefficient is specified as 0.43 based on Eq. (41) as well as on experimental results of several durability tests

[28–32]. The constraint functions for strength requirement $\Phi^1 \sim \Phi^3$ thus can be presented as Eqs. (65)–(67).

$$\Phi^1 = \begin{cases} |\bar{\epsilon}_{fl}^x| \leq 0.43c\epsilon^u \\ |\bar{\epsilon}_{fl}^y| \leq 0.43c\epsilon^u \end{cases} \quad (64)$$

$$\Phi^2 = \begin{cases} |\bar{\epsilon}_{fl}^x| \leq 0.43t\epsilon^u \\ |\bar{\epsilon}_{fl}^y| \leq 0.43c\epsilon^u \end{cases} \quad (65)$$

$$\Phi^3 = |\bar{\gamma}_w^{xy}| \leq 0.43s\gamma^u \quad (66)$$

The Chinese design specifications of highway bridges [24] recommended that the bridge deck transverse deflection should be smaller than the girder’s span (b) divided by 400 (i.e. $b/400$). The constraint functions for stiffness requirement thus should be expressed as:

$$\Phi^4 = \delta_f^{z(max)} \leq b/400 \quad (67)$$

The 0°-lamina of pultruded GFRP laminates is in the form of E-glass roving, while both the 90°- and ± 45°-laminates are in the form of stitched E-glass fabrics. Due to the limitation of pultrusion manufacturing process, the contents of roving are much larger than fabrics for guaranteeing necessary pultrusion traction, making the content of 0° lamina is much larger than the laminas with other angle orientations [15]. The minimum ratio of 0° lamina is specified as 50% to guarantee necessary pultrusion traction, and the maximum ratio of 90° and ± 45° lamina is set as 20% considering manufacture difficulties with larger fabric content. Then constrain functions for pultrusion manufacture requirement is specified by Eq. (68).

$$\Phi^5 = \begin{cases} 0.25 \leq V_f \leq 0.70 \\ 0.5 \leq \xi_0 \leq 0.95 \\ 0.05 \leq \xi_{45} \leq 0.2 \\ 0.05 \leq \xi_{90} \leq 0.2 \end{cases} \quad (68)$$

To avoid local buckling and consider manufacturing capabilities and limitations, a maximum height of the GFRP bridge deck is set to 300 mm, the maximum flange thickness is set as 50 mm, and the maximum web thickness per meter is assumed as 250 mm. The constraint functions for geometry requirements are specified as in Eq. (69) as follow:

$$\Phi^6 = \begin{cases} 5 \leq t_u \leq 50 \\ 5 \leq t_l \leq 50 \\ 5 \leq t_w \leq 250 \\ 50 \leq h_w \leq 300 \end{cases} \quad (69)$$

The optimization process was achieved by minimizing ϕ_1 or ϕ_2 under the constraint Φ^1 - Φ^6 using constrained nonlinear minimization (fmincon) function in the MATLAB™ software [33]. The optimized two-scale parameters of this case study are listed in Table 3. It can be seen that the weight objective function ϕ_1 and the price objective function ϕ_2 also calculate the same results. This is mainly because that the stiffness

Table 3
Optimized two-scale parameters of case study.

Item	Unit	Price Optimization	Weight Optimization
Top flange thickness t_u	mm	46.02	46.02
Bottom flange thickness t_l	mm	45.86	45.86
Web height, h_w	mm	300.0	300.0
Web thickness per meter, t_w	mm	37.42	37.42
Ratio of 0° lamina, ξ_0	–	0.779	0.779
Ratio of 45° lamina, ξ_{45}	–	0.171	0.171
Ratio of 90° lamina ξ_{90}	–	0.050	0.050
Fiber volume fraction, V_f	–	0.652	0.652
Price per square meter, φ_1	RMB	2025.9	2025.9
Weight per square meter, φ_2	kg	213.7	213.7

requirement (constrain function ϕ^4) is most strict based on the specification of steel or concrete deck among all the constrained functions. The optimized top flange thickness t_{ts} , bottom flange thickness t_b , web height h_w , web thickness per meter t_w are 46.02 mm, 45.86 mm, 300 mm and 37.42 mm. Also, the optimized ratio of the 0° -lamina, the 45° -lamina, and the 90° -lamina are 77.9%, 17.1%, 5.0%. The optimized fiber volume fraction is 65.2%. The optimized parameters are the same in terms of price and weight optimization because the governing factor is the web height.

8. Conclusions

The optimization process described in this paper involves identifying the optimal ratio of reinforcements (roving and/or fabric), fiber volume fractions, in conjunction with geometrical variables in order to achieve the optimum design in both material and structure scales. In this paper, the macro behaviors of pultruded FRP bridge deck are analyzed based on the design specification of the highway bridge. The equivalent properties of the pultruded GFRP lamination are calculated by combining both micromechanics and classical lamination theory. The micro fiber/resin level is bridged to macro pultruded GFRP bridge level by assuming the effective strain homogenized from micro component equals to macro strain. The multiscale lamination optimization is achieved by finding optimized two-scale design parameters for minimizing bridge weight and/or materials and construction cost while satisfying all design parameters for the pultruded composite deck. The optimized two-scale parameters were obtained by solving the proposed multiscale optimization model, for a bridge with a main span of 20.0 m and steel girders equal spacing of 3.0 m. The optimized values of the top flange thickness, t_{ts} , the bottom flange thickness, t_b , the web height, h_w , and the web thickness per meter, t_w , are 46.02 mm, 45.86 mm, 300.0 mm and 37.42 mm, respectively. Results also showed that the optimized ratio of the 0° -lamina, 45° -lamina, and the 90° -lamina are 77.9%, 17.1%, 5.0%. The optimized fiber volume fraction is 65.2%.

Declaration of Competing Interest

The authors declare that they have no known competing financial interests or personal relationships that could have appeared to influence the work reported in this paper.

Acknowledgments

The authors gratefully acknowledge the financial support provided by the National Natural Science Foundation (Grants #51808398 & 51578406) of the People's Republic of China. The author José A.F.O. Correia would like to acknowledge the support given by base funding - UIDB/04708/2020 and programmatic funding - UIDP/04708/2020 of the CONSTRUCT - Instituto de I&D em Estruturas e Construções - funded by national funds through the FCT/MCTES (PIDDAC).

References

- [1] Bank LC. *Compos Constr* 2006. <https://doi.org/10.1002/9780470121429>.
- [2] Mosallam AS, Bayraktar A, Elmikawi M, Pul S, Adanur S. *Polymer Composites in Construction. An Overview*; 2014.
- [3] Xin H, Mosallam A, Liu Y, Xiao Y, He J, Wang C, et al. Experimental and numerical investigation on in-plane compression and shear performance of a pultruded GFRP composite bridge deck. *Compos Struct* 2017;180:914–32.
- [4] Xin H, Mosallam AS, Liu Y, Wang C, He J. Experimental and numerical investigation on assessing local bearing behavior of a pultruded GFRP bridge deck. *Compos Struct* 2018;204:712–30.
- [5] Zuo Y, Mosallam A, Xin H, Liu Y, He J. Flexural performance of a hybrid GFRP-concrete bridge deck with composite T-shaped perforated rib connectors. *Compos Struct* 2018;194:263–78.
- [6] Xin H, Mosallam A, Liu Y, Wang C, Zhang Y. Analytical and experimental evaluation of flexural behavior of FRP pultruded composite profiles for bridge deck structural design. *Constr Build Mater* 2017;150:123–49. <https://doi.org/10.1016/j.conbuildmat.2017.05.212>.
- [7] Zou X, Feng P, Bao Y, Wang J, Xin H. Experimental and analytical studies on shear behaviors of FRP-concrete composite sections. *Eng Struct* 2020;215:110649.
- [8] Xiong Z, Liu Y, Zuo Y, Xin H. Experimental evaluation of shear behavior of pultruded GFRP perforated connectors embedded in concrete. *Compos Struct* 2019;222:110938.
- [9] Zhang Y, Mosallam A, Liu Y, Sun Y, Xin H, He J. Assessment of flexural behavior of pultruded GFRP laminates for bridge deck applications. *Adv Mater Sci Eng* 2019;2019.
- [10] Xiong Z, Liu Y, Zuo Y, Xin H. Shear performance assessment of sand-coated GFRP perforated connectors embedded in concrete. *Materials (Basel)* 2019;12:1906.
- [11] Nijgh MP, Xin H, Veljkovic M. Non-linear hybrid homogenization method for steel-reinforced resin. *Constr Build Mater* 2018;182:324–33.
- [12] He J, Wang S, Liu Y, Wang D, Xin H. Shear behavior of steel I-girder with stiffened corrugated web. Part II: Numerical study. *Thin-Walled Struct*; 2020. p. 147.
- [13] Mosallam A. *Design guide for FRP Composite Connections* 2011. <https://doi.org/10.1061/9780784406120>.
- [14] Xin H, Mosallam A, Liu Y, Veljkovic M, He J. Mechanical characterization of a unidirectional pultruded composite lamina using micromechanics and numerical homogenization. *Constr Build Mater* 2019;216:101–18.
- [15] Xin H, Liu Y, Mosallam AS, He J, Du A. Evaluation on material behaviors of pultruded glass fiber reinforced polymer (GFRP) laminates. *Compos Struct* 2017;182:283–300. <https://doi.org/10.1016/j.compstruct.2017.09.006>.
- [16] Kathiravan R, Ganguli R. Strength design of composite beam using gradient and particle swarm optimization. *Compos Struct* 2007;81:471–9.
- [17] Nikbakt S, Kamarian S, Shakeri M. A review on optimization of composite structures Part I: Laminated composites. *Compos Struct* 2018.
- [18] Johansen L, Lund E. Optimization of laminated composite structures using determination criteria and hierarchical models. *Struct Multidiscip Optim* 2009;38:357–75.
- [19] Park JH, Hwang JH, Lee CS, Hwang W. Stacking sequence design of composite laminates for maximum strength using genetic algorithms. *Compos Struct* 2001;52:217–31.
- [20] Scares CMM, Soares CAM, Correia VMF. Optimization of multilaminated structures using higher-order deformation models. *Comput Methods Appl Mech Eng* 1997;149:133–52.
- [21] Zou B, Chen A, Davalos JF, Salim HA. Evaluation of effective flange width by shear lag model for orthotropic FRP bridge decks. *Compos Struct* 2011;93:474–82. <https://doi.org/10.1016/j.compstruct.2010.08.033>.
- [22] Davalos JF, Chen A, Zou B. Performance of a scaled FRP deck-on-steel girder bridge model with partial degree of composite action. *Eng Struct* 2012;40:51–63. <https://doi.org/10.1016/j.engstruct.2012.02.020>.
- [23] Offals T. *AASHTO LRFD bridge design guide specifications for GFRP-reinforced concrete bridge decks and traffic railings*. AASHTO 2009.
- [24] D60 JTG. *General Code for Design of Highway Bridges and Culverts* 2004.
- [25] Timoshenko SPX. *On the transverse vibrations of bars of uniform cross-section*. London, Edinburgh, Dublin Philos Mag J Sci 1922;43:125–31.
- [26] Barbero EJ. *Introduction to composite materials design*. CRC Press; 2017.
- [27] Soden PD, Hinton MJ, Kaddour AS. Lamina properties, lay-up configurations and loading conditions for a range of fibre reinforced composite laminates. *Fail Criteria Fibre-Reinforced-Polymer Compos* 2004;58:30–51. <https://doi.org/10.1016/B978-008044475-8/50003-2>.
- [28] Xin H, Mosallam A, Liu Y, Wang C, Zhang Y. Impact of hygrothermal aging on rotational behavior of web-flange junctions of structural pultruded composite members for bridge applications. *Compos Part B Eng* 2017;110:279–97. <https://doi.org/10.1016/j.compositesb.2016.09.105>.
- [29] Xin H, Liu Y, Mosallam A, Zhang Y. Moisture diffusion and hygrothermal aging of pultruded glass fiber reinforced polymer laminates in bridge application. *Compos Part B* 2016;100:197–207. <https://doi.org/10.1016/j.compositesb.2016.04.085>.
- [30] Xin H, Mosallam A, Liu Y, Wang C. Hygrothermal aging effects on axial behaviour of pultruded web-flange junctions and adhesively bonded build-up bridge members. *J Reinf Plast Compos* 2018;37:13–34.
- [31] Xin H, Mosallam A, Liu Y, Yang F, Zhang Y. Hygrothermal aging effects on shear behavior of pultruded FRP composite web-flange junctions in bridge application. *Compos Part B* 2017;110:213–28. <https://doi.org/10.1016/j.compositesb.2016.10.093>.
- [32] Xin H, Liu Y, Mosallam A, Zhang Y, Wang C. Hygrothermal aging effects on flexural behavior of pultruded glass fiber reinforced polymer laminates in bridge applications. *Constr Build Mater* 2016;127:237–47. <https://doi.org/10.1016/j.conbuildmat.2016.09.151>.
- [33] Guide MU. *The mathworks. Inc, Natick, MA* 1998;5:333.